

# Aligned Divergent Pathways for Omni-Domain Generalized Person Re-identification

Eugene P.W. Ang

Rapid-Rich Object Search (ROSE) Lab  
Nanyang Technological University  
Singapore, Singapore  
phuaywee001@e.ntu.edu.sg

Shan Lin

Rapid-Rich Object Search (ROSE) Lab  
Nanyang Technological University  
Singapore, Singapore  
shan.lin@ntu.edu.sg

Alex C. Kot

Rapid-Rich Object Search (ROSE) Lab  
Nanyang Technological University  
Singapore, Singapore  
eackot@ntu.edu.sg

**Abstract**—Person Re-identification (Person ReID) has advanced significantly in fully supervised and domain generalized Person ReID. However, methods developed for one task domain transfer poorly to the other. An ideal Person ReID method should be effective regardless of the number of domains involved in training or testing. Furthermore, given training data from the target domain, it should perform at least as well as state-of-the-art (SOTA) fully supervised Person ReID methods. We call this paradigm *Omni-Domain Generalization Person ReID*, referred to as ODG-ReID, and propose a way to achieve this by expanding compatible backbone architectures into multiple diverse pathways. Our method, Aligned Divergent Pathways (ADP), first converts a base architecture into a multi-branch structure by copying the tail of the original backbone. We design our module Dynamic Max-Deviance Adaptive Instance Normalization (DyMAIN) that encourages learning of generalized features that are robust to omni-domain directions and apply DyMAIN to the branches of ADP. Our proposed Phased Mixture-of-Cosines (PMoC) coordinates a mix of stable and turbulent learning rate schedules among branches for further diversified learning. Finally, we realign the feature space between branches with our proposed Dimensional Consistency Metric Loss (DCML). ADP outperforms the state-of-the-art (SOTA) results for multi-source domain generalization and supervised ReID within the same domain. Furthermore, our method demonstrates improvement on a wide range of single-source domain generalization benchmarks, achieving Omni-Domain Generalization over Person ReID tasks.

**Index Terms**—Person Re-identification, Domain Generalization, Omni-Domain Generalization

## I. INTRODUCTION

Person Re-identification (ReID) matches the image of a query person with other images captured in other nonoverlapping cameras. The simplest fully supervised single-domain ReID tasks train and test within a single domain of cameras, whereas in domain generalized ReID (DG-ReID), training and test sets come from mutually exclusive camera domains. The best single-domain ReID methods perform significantly worse when tested on other unseen domains, but the same problem exists in the other direction for methods specialized in domain generalization: overspecialization to the generalization task also affects performance in the simple single domain

setting. Illustrated in Table I, a baseline single domain ResNet-50 method [1] performs much worse than specialized DG-ReID methods when evaluated across domains. However, even when provided with samples from the test domain for training, these state-of-the-art (SOTA) methods specialized in DG-ReID *severely underperform a simple baseline*, suggesting that these methods are overly specialized for the generalization task. An ideal Person ReID method that has truly learnt to generalize should do as well, if not better, when trained with data from the test domain. We call this paradigm *Omni Domain Generalization Person Re-identification*, referred to as ODG-ReID. In this work, we introduce our solution, Aligned Divergent Pathways (ADP), that is agnostic to the above domain configuration changes and can achieve ODG-ReID.

TABLE I: The performance of single-domain methods degrades when testing on other datasets, while cross-domain generalization methods cannot maintain the same performance on the original training dataset. Dataset abbreviations: M is Market-1501 [2], D is DukeMTMC-reID [3], C is CUHK03 [4], and MS is MSMT17\_V2 [5]. Dataset(s) on the left side of the arrow are used in training and evaluation is performed on the dataset on the right. All results are in mAP and the best result for each benchmark is bold.

| Setting            | Methods            | Single Domain Train |             | Multi-Domain Train |             |
|--------------------|--------------------|---------------------|-------------|--------------------|-------------|
|                    |                    | D → D               | M → D       | C+D+M → D          | C+M+MS → D  |
| Normal             | Baseline (BoT) [1] | <b>76.3</b>         | 16.1        | <b>76.3</b>        | 38.6        |
|                    | DualNorm [6]       | 67.7                | 23.9        | 76.3               | 40.5        |
| Domain Generalized | META [7]           | 46.7                | 18.3        | 60.6               | 42.7        |
|                    | ACL [8]            | 49.9                | 22.2        | 72.9               | <b>53.4</b> |
|                    | SIL [9]            | 61.5                | <b>25.1</b> | 65.6               | 47.0        |

Given a standard backbone architecture such as a ViT [10] or ResNet [11], our framework expands the backbone with branches by making multiple tail copies. We add our proposed normalization method, Dynamic Max-Deviance Adaptive Instance Normalization (DyMAIN) to each branch, which infuses *maximal style variation* into each data batch, cross-pollinating styles between pairs that are most different in style from one another. This encourages the learning of generalized features that are robust to omni-domain generalization settings.

Next, our Phased Mixture-of-Cosines (PMoC) learning rate schedules coordinate a diverse mix of schedules among the branches, from stable schedules with small learning rates and long cycles, to turbulent schedules with large learning rates and short cycles.

arXiv:2410.08466v1 [cs.CV] 11 Oct 2024

Finally, we propose a novel metric learning loss, Dimensional Consistency Metric Loss (DCML), that enforces alignment between the inter-pathway feature dimensions. ADP outperforms SOTA multi-source domain generalization and single-domain supervised ReID benchmarks, demonstrating omni-domain generalization. Furthermore, we show in our ablation studies that the components of ADP improve performance on many single-source domain generalization benchmarks.

Our contributions are summarized as follows:

- We investigate Omni-Domain Person Re-identification, referred to as ODG-ReID, demonstrating that single domain methods cross domains ineffectively, while DG-ReID methods perform poorly in settings where test domain samples are provided for training. ODG-ReID is a crucial capability in real-world applications but, to the best of our knowledge, is rarely considered.
- We propose a novel and highly adaptable framework, ADP, that can be applied on popular backbone architectures such as ViTs and ResNets.
- ADP outperforms SOTA Person ReID performance in multi-source generalization and single-domain benchmarks. Furthermore, we demonstrate improvements on a wide range of single-source domain generalization tasks.

## II. RELATED WORK

**Single-Domain Person Re-identification** Single-domain ReID SOTA methods are mostly based on deep convolutional neural networks. Early deep learning based work usually formulated Person ReID as a verification problem and proposed Siamese architectures [4], [12], [13]. Then, verification-driven triplet architectures, such as [14], [15] overtook Siamese structures to add robustness. Zheng et al. [16] first proposed the widely adopted ID-Discriminative embedding (IDE) to train models pretrained on ImageNet [17] to classify person IDs. More recent approaches [1], [18], [19] combine classification and verification losses.

**Domain-Generalized Person ReID:** DG-ReID aims to learn a model that can generalize well to unseen target domains without using any target domain data for training. Instance normalization (IN) was used to normalize style variation [20] and is particularly successful in DG-ReID [6]. Adaptive IN (AdaIN) [21] extends this concept by mixing style features from an image with the content features of a target image. Our proposed normalization, DyMAIN, extends AdaIN to select style sources based on maximal deviance. MMFA-AAE [22] used a domain adversarial learning approach to remove domain-specific features. QAConv [23] and M<sup>3</sup>L [24] used meta-learning frameworks coupled with memory bank strategies. DEX [25] proposed a domain-based implicit semantic augmentation loss function to learn domain invariant features. ACL [8] proposed a module to separately process domain invariant and domain specific features, plugging the module to replace selected convolutional blocks. RaMoE [26] and META [7] deploy a mixture of experts to specialize to each domain. Style Interleaved Learning (SIL) [9] is a

framework with a regular forward/backward pass, with one additional forward pass that employs style interleaving on features to update class centroids. The recent development of Vision Transformers (ViT) [10] birthed a new generation of DG-ReID methods using ViT backbones. For instance, Part-Aware Transformer [27] learns locally similar features shared across different IDs, further using the part-guided information for self-distillation.

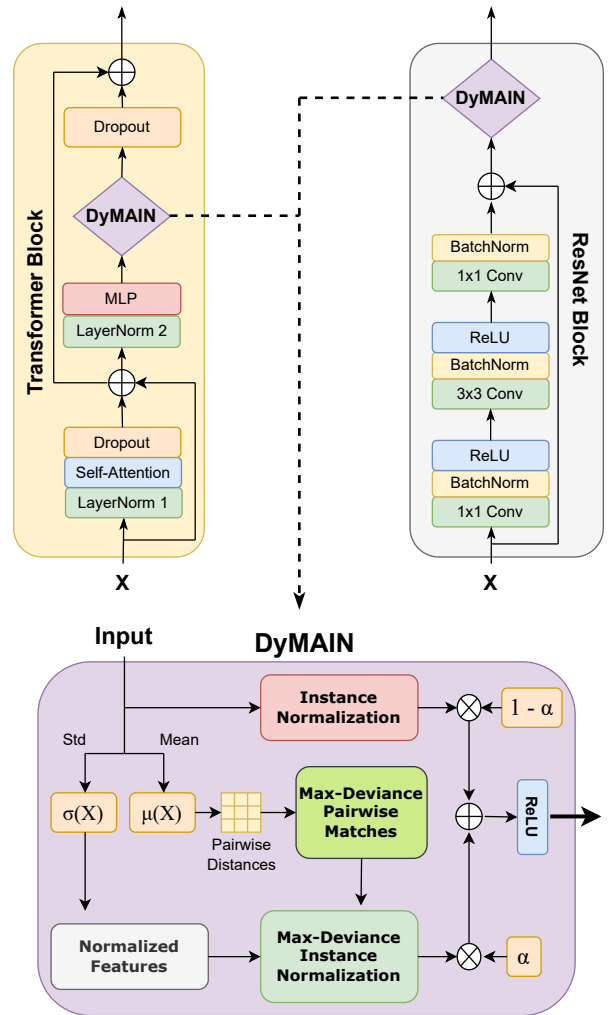


Fig. 1: DyMAIN can be applied on Transformer and ResNet blocks. The internal structure of our DyMAIN module is illustrated in detail in the flow-diagram at the bottom of the figure.

## III. METHODOLOGY

### A. Preliminaries

We are given a dataset of person images with identity labels  $D = \{x_i, y_i\}_1^n$ . For ViT backbones, we sample the image  $x_i$  in a grid, linearize them into a sequence of image patches which we embed into a sequence of features. We then append a class token to the front of the sequence and add positional encodings to preserve the embedding order. We notate a batch of such sequences as  $X \in \mathbb{R}^{N, S, d}$ , where  $N$  is batch size,  $S$  is the sequence length (class token plus number of image

patches) and  $d$  is the embedding dimension.  $X$  forms the input to a series of transformer encoder blocks that further specialize the sequence of encodings for relevant tasks. At the end of the encoder blocks, the class token is used for training or inference. For ResNets, we follow well established standards [1].

### B. Dynamic Max-Deviance Adaptive Instance Normalization

DyMAIN is illustrated in Fig 1. Given a batch of inputs  $X$  we compute the feature-wise means  $\mu(X)$  and standard deviations  $\sigma(X)$ , which we use to normalize the inputs:  $\bar{X}_i = \frac{X_i - \mu(X_i)}{\sqrt{\sigma_i^2(X_i) + \epsilon}}$  where  $\epsilon$  is a small value for numerical stability. Further, we compute the pairwise distances between the feature means  $\mu(X)$  and use it to match batch samples: each sample  $X_i$  is paired with its most distant counterpart  $X_{M_i}$  to derive a set of matchings  $\{i, M_i\}_{i=1}^N$ . For our Max-Deviance Adaptive Instance Normalization (MAIN), we mix the style feature of sample  $X_{M_i}$  into its paired content feature  $X_i$ :  $\text{IN}_{MA}(X_i) = (\frac{X_i}{\sigma(X_{M_i})} + \mu(X_{M_i}))\gamma + \beta$  where  $\gamma$  and  $\beta$  are learnable affine parameters. DyMAIN combines MAIN with regular Instance Normalization as  $\text{IN}_{DyMA}(X) = \sum_{i=1}^N \alpha \text{IN}_{MA}(X_i) + (1 - \alpha) \text{IN}(X_i)$ , using a learnable parameter  $\alpha \in \mathbb{R}^d$  that combines the outputs of both normalizations along the embedding dimension.

### C. Phased Mixture-of-Cosines

While cosine learning rate schedulers are effective in the training of deep neural networks, using the same scheduler in all branches overly correlates their performance as all go through the same stages of learning at the same time. We apply different schedules to each branch so that they explore different feature spaces at each point in time, collectively providing the model with divergent opinions. Fig 2a illustrates a normal learning rate schedule. We deploy a mix of turbulent schedules with larger learning rates but shorter periods and stable schedules with smaller learning rates and longer periods. Formally, given total epochs  $T$ , minimum learning rate  $\eta_{min}$ , learning rate power factor  $\gamma$ , target decay factor  $\lambda$ , each branch  $k$  with period  $p_k$  epochs trains for  $c_k = \lfloor \frac{T}{p_k} \rfloor$  cycles with a base learning rate of  $\eta_k = (c_k)^\gamma \eta_{min}$ . After each cycle, we decay the learning rate by a factor of  $\lambda^{\frac{1}{c_k}}$ . Fig 2b illustrates example schedules that run multiple cycles with learning rate decay between cycles.

### D. Aligned Divergent Pathways

Figure 3 illustrates our method, ADP. The final blocks of the backbone spawn multiple branches that share the earlier layers for a more parameter-efficient architecture. Each branch is specialized with DyMAIN, allowing them to learn features with maximum style variation. Each branch explores different embedding space-time combinations due to the coordination of unique learning rate schedules from our PMoC scheduler. We apply DCML loss to encourage the features among sibling branches to be consistent and aligned. At the end of the inference pass, we combine all branch features together by taking the mean along the feature dimension.

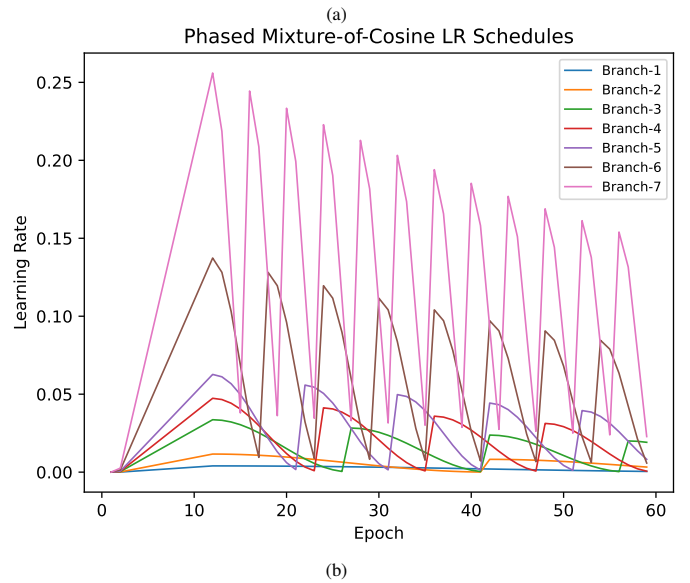
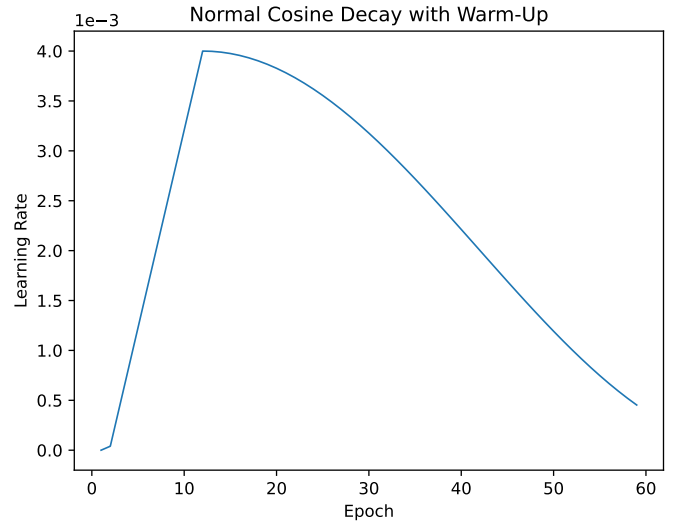


Fig. 2: Comparing a standard cosine learning rate schedule (a) with our ensemble of Phased Mixture-of-Cosine (PMoC) schedulers. The mix of turbulent and stable schedules in PMoC encourages learning diverse features among different branches.

### E. Dimensional Consistency Metric Loss

The diverse learning rate schedules coordinated by PMoC results in a larger exploration space between branches, but a balance needs to be achieved between exploration and consistency. We propose our DCML loss to keep inter-branch distances small and also encourage features to be more aligned in feature dimension. Given  $\{X_i := f_i(X)\}_{i=1}^k$ , a set of sibling feature outputs from  $k$  branches (each denoted by a function  $f_i$ ), we compute the Chebyshev distance between any pair of features  $(x, y)$ :  $D_\infty(x, y) = \max_i(|x_i - y_i|)$ . Dimensional consistency is encouraged by reducing the *maximum component difference* between each pair of inter-branch

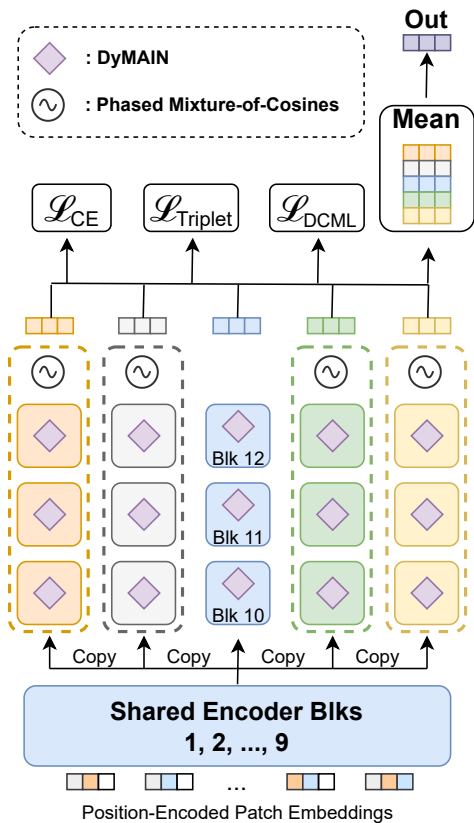


Fig. 3: A summary of our method, ADP. Image inputs are processed into sequences of patches and passed through a backbone model, such as a Vision Transformer. The final blocks of the backbone are cloned to make a self-ensemble of several branches. Our own normalization module DyMAIN is added to all branch blocks, and each branch specialized with a different cosine learning rate schedule via Phased Mixture-of-Cosines. A dimensional consistency metric loss (DCML) is imposed to further align the features from different branches.

features, resulting in our DCML loss function:

$$\mathcal{L}_{DCML}(X) = \frac{1}{\binom{k}{2}} \sum_{(i,j) \in \binom{1..k}{2}} D_{\infty}(X_i, X_j) \quad (1)$$

Other metrics such as Manhattan or Euclidean distances densely penalize deviations between all the dimensions of two input vectors. Such metrics degrade the final performance of the model.  $\mathcal{L}_{DCML}$ , on the other hand, only penalizes component with the maximum absolute deviation and its sparsity helps with learning of generalized and aligned sibling features.

#### F. Loss Functions

For a batch of input samples  $X$  with labels  $y$ , ADP generates output features from  $k$  branches  $\{f_i(X)\}_{i=1}^k$ . We apply a per-branch cross-entropy loss over the person identity labels:

$$\mathcal{L}_{CE}^b(X, y) = -\log \frac{\exp \mathbf{w}_y^b \cdot f_b(X)}{\sum_{j=1}^C \exp \mathbf{w}_j^b \cdot f_b(X)}, \quad (2)$$

where  $\mathbf{w}^b$  are branch classifier weights, and  $C$  is the total number of classes. We also apply triplet losses per-branch:

$$\mathcal{L}_{Tri}^b(X) = \sum_{(a,p,n) \in T(f_b(X))} [d_{a,p} - d_{a,n} + m]_+, \quad (3)$$

where  $d$  is a distance metric,  $m \in \mathbb{R}$  is a margin parameter and  $a, p, n$  are anchor, positive and negative triplets mined from  $f_b(X)$  using a triplet collator  $T$  such as hard-example mining [14]. Adding our DCML, the overall loss is a weighted sum of the three individual losses balanced by hyperparameters  $0 \leq w_1, w_2, w_3$ :

$$L_{ADP}(X) = \sum_{b=1}^k [w_1 \mathcal{L}_{CE}^b(X) + w_2 \mathcal{L}_{Tri}^b(X)] + w_3 \mathcal{L}_{DCML}(X) \quad (4)$$

## IV. EXPERIMENTS

### Person ReID Datasets and Multi-Source Domain Generalization Benchmarks

For multi-source DG-ReID benchmarks we adopt a leave-one-out evaluation where out of four datasets, Market-1501 (M), DukeMTMC-reID (D), CUHK03 (C) and MSMT17\_V2 (MS), three are used for training and one for testing, e.g. D+M+MS means that we train on D, M and MS and test on C. For CUHK03 we use the new partition, following [25]. Only the training sets of the source domains are used in training.

**Single Domain ReID Benchmarks** The single domain benchmarks use the same ReID datasets (M, D, C and MS). In supervised ReID, we use the same dataset for training and testing. For single-source DG-ReID, we use the training split of a dataset for training and evaluate on the test split of another dataset. For CUHK03, to align our results those reported by SOTA single-domain methods, we use the classic split with detected bounding boxes.

We evaluate all methods with mean average precision (mAP) and Rank-1.

#### A. Implementation Details

We apply ADP on two backbones, ViT-b-16 [10] and ResNet-50 [11], both with weights pretrained on ImageNet [17]. Input images are resized into 384x128 pixels. For ViT, patches of 16x16 pixels are sampled from the image in strides of 12, then linearized and position-encoded into a sequence of  $\mathbb{R}^{768}$  embeddings. For both backbones we clone the last four blocks/bottlenecks to make each branch, creating a total of  $k=7$  branches. DyMAIN is applied to all blocks of each branch. Our cross-entropy, triplet and DCML losses have weights of  $w_1 = 1, w_2 = 1, w_3 = 0.01$ . We use a SGD optimizer with a base learning rate of  $\eta = 0.004$  and momentum 0.9. The main branch uses a cosine learning rate schedule, warming up linearly over ten epochs starting from  $0.01\eta$  and attenuating over the course of training in one cycle, down to a minimum learning rate of  $0.002\eta$ . For PMoC, we set  $\eta_{min} = 0.004, \gamma = 1.806, \lambda = 0.5$  and the branches cycle in periods of  $p_{1..k} = [120, 60, 30, 24, 20, 15, 12]$  epochs respectively. We use a batch size of 64 and apply auto-augmentation [29] with  $p = 0.1$ . For each encoder block, we apply dropout with  $p = 0.1$ . We train for a total of 120 epochs ( $T = 120$ ).

TABLE II: Results on the modern DG-ReID benchmarks. For the methods with the dagger symbol †, we evaluated the official open source implementation on this benchmark. **Bold** numbers are the best, while underlined numbers are second. Ours (R50) is our method with the ResNet-50 backbone, while Ours (ViT) is with the Vision Transformer backbone.

| Method                | C+D+MS→M    |             | C+M+MS→D    |             | C+D+M→MS    |             | D+M+MS→C    |             |
|-----------------------|-------------|-------------|-------------|-------------|-------------|-------------|-------------|-------------|
|                       | Rank-1      | mAP         | Rank-1      | mAP         | Rank-1      | mAP         | Rank-1      | mAP         |
| DualNorm [6] †        | 78.9        | 52.3        | 68.5        | 51.7        | 37.9        | 15.4        | 28.0        | 27.6        |
| QAConv [23]           | 67.7        | 35.6        | 66.1        | 47.1        | 24.3        | 7.5         | 23.5        | 21.0        |
| OSNet-IBN [28] †      | 73.4        | 45.1        | 61.5        | 42.3        | 35.7        | 13.7        | 20.9        | 20.9        |
| OSNet-AIN [28] †      | 74.2        | 47.4        | 62.7        | 44.5        | 37.9        | 14.8        | 22.4        | 22.4        |
| M <sup>3</sup> L [24] | 75.9        | 50.2        | 69.2        | 51.1        | 36.9        | 14.7        | 33.1        | 32.1        |
| DEX [25]              | 81.5        | 55.2        | 73.7        | 55.0        | 43.5        | 18.7        | 36.7        | 33.8        |
| SIL [9] †             | 79.2        | 52.8        | 68.3        | 47.0        | 36.9        | 13.8        | 29.5        | 28.9        |
| META [7] †            | 66.7        | 44.6        | 61.8        | 42.7        | 32.4        | 13.1        | 21.3        | 21.6        |
| ACL [8] †             | 86.1        | <u>63.1</u> | 71.7        | 53.4        | 47.2        | 19.4        | 35.5        | 34.6        |
| Ours (R50)            | <u>86.3</u> | <u>62.0</u> | <u>76.5</u> | <u>58.9</u> | <u>48.3</u> | 21.2        | <u>38.4</u> | <u>37.6</u> |
| PAT [8]               | 75.2        | 51.7        | 71.8        | 56.5        | 45.6        | <u>21.6</u> | 31.1        | 31.5        |
| Ours (ViT)            | <b>86.6</b> | <b>64.5</b> | <b>77.4</b> | <b>62.4</b> | <b>53.4</b> | <b>25.7</b> | <b>41.6</b> | <b>40.7</b> |

TABLE III: Results on the Single Domain ReID Benchmarks. For the methods with the dagger symbol †, we evaluated the official open source implementation on this benchmark. **Bold** numbers are the best, while underlined numbers are second. Ours (R50) is our method with the ResNet-50 backbone, while Ours (ViT) is with the Vision Transformer backbone.

| Method               |     | Single-Domain |       |             | Domain Generalization |       |        |       | Omni-Domain Generalization |             |             |
|----------------------|-----|---------------|-------|-------------|-----------------------|-------|--------|-------|----------------------------|-------------|-------------|
|                      |     | BoT †         | MGN † | AGW         | DualNorm †            | SIL † | META † | ACL † | OSNet-AIN †                | Ours (R50)  | Ours (ViT)  |
| <b>Market-1501</b>   | mAP | 80.6          | 85.3  | <u>88.2</u> | 76.4                  | 71.9  | 47.2   | 73.1  | 78.5                       | 87.6        | <b>88.5</b> |
|                      | R1  | 92.3          | 94.5  | <b>95.3</b> | 91.9                  | 88.9  | 75.1   | 88.0  | 92.5                       | 95.0        | <u>95.1</u> |
| <b>DukeMTMC-reID</b> | mAP | 63.0          | 76.3  | <b>79.6</b> | 67.7                  | 61.5  | 46.7   | 49.9  | 69.9                       | 78.6        | <u>79.5</u> |
|                      | R1  | 78.9          | 86.9  | 89.0        | 83.8                  | 79.9  | 73.1   | 71.5  | 84.7                       | 89.5        | <u>89.1</u> |
| <b>CUHK03</b>        | mAP | 88.5          | 87.6  | 62.0        | 67.2                  | 78.1  | 56.0   | 79.8  | 70.0                       | <b>89.9</b> | <u>89.7</u> |
|                      | R1  | 90.5          | 91.1  | 63.6        | 68.9                  | 82.5  | 60.5   | 83.2  | 74.9                       | <b>93.0</b> | <u>92.8</u> |
| <b>MSMT17 (V2)</b>   | mAP | 49.2          | 50.5  | 49.3        | 43.9                  | 37.2  | 37.1   | 27.7  | 42.7                       | <u>61.0</u> | <b>62.0</b> |
|                      | R1  | 74.7          | 74.8  | 68.3        | 74.4                  | 66.2  | 69.1   | 57.0  | 71.5                       | <u>83.8</u> | <b>85.0</b> |

## B. Results on Cross Domain Generalization ReID

Table II presents a comparison between our ADP and other DG-ReID methods on the modern leave-one-out benchmarks. ADP improves the domain generalization performance of the ViT backbone, outperforming recent SOTA methods by a considerable margin - our method surpasses the previous SOTA by 5.9% in mAP for C+M+MS → D, by 4.1% in mAP and 6.2% in Rank-1 for C+D+M → MS and by 6.1% in mAP and 4.9% in Rank-1 for D+M+MS → C. ADP also improves the capability of the ResNet-50, surpassing nearly all other similar methods based on the same backbone.

## C. Results on Single Domain ReID benchmarks

Table III compares ADP against SOTA DG-ReID and single domain ReID methods. SOTA DG-ReID methods perform worse on single domain tasks because of over-specialization to domain generalization tasks. In contrast, ADP reaches SOTA-level performance in all four single domain ReID benchmarks, even outperforming previous SOTA methods by 11.5% in mAP and by 10.2% in Rank-1 for the MSMT17 benchmark.

## D. Ablation Studies

We conduct ablation experiments to find the best hyperparameter configurations of each of its components. For brevity, we only report results of ADP on the ViT backbone. Through

these experiments, we show that the components improve a wide range of single-source DG-ReID benchmarks.

1) *Ablation over application of DyMAIN*: Table IV shows how DyMAIN improves domain generalization for selected benchmarks MS → M and M → C. Starting from a vanilla ViT control, we progressively add DyMAIN to an increasing number of ending transformer encoder blocks. Performance improves steadily by nearly 2% Rank-1 and mAP when we apply DyMAIN on up to four of the ending blocks. We observe that adding DyMAIN to more than the last four blocks begins to degrade performance.

TABLE IV: Ablation over application of DyMAIN. We experiment on a single-branch base model and gradually increase the number of ending blocks that we apply DyMAIN to.

| Blocks Applied | MS → M      |             | M → C       |             |
|----------------|-------------|-------------|-------------|-------------|
|                | mAP         | R1          | mAP         | R1          |
| <b>None</b>    | 46.6        | 72.5        | 26.6        | 25.4        |
| <b>1</b>       | 47.5        | 73.2        | 26.9        | 25.9        |
| <b>2</b>       | 47.7        | 73.6        | 26.8        | 25.7        |
| <b>3</b>       | 47.6        | 72.7        | 26.9        | 26.2        |
| <b>4</b>       | <b>48.4</b> | <b>73.9</b> | <b>27.6</b> | <b>27.1</b> |
| <b>5</b>       | 47.9        | 73.2        | 26.5        | 25.4        |

2) *Comparing learning rate schedules:* We compare our PMoC (with implementation details as described in Subsection IV-A) against a stable learning rate schedule (Stable) where all branches apply the same cosine schedule with  $\eta = 0.004$  over a single period. To ensure that a higher base learning rate is not the cause behind the improvement, we compare these two experiments against a learning rate schedule where all branches apply a high base learning rate of  $\eta = 0.256$  (Turbulent). Table V shows that diversity of learning rate schedules result in significant performance gains of around 2% on the single-source domain generalization benchmarks  $MS \rightarrow C$  and  $M \rightarrow D$ .

TABLE V: Comparing PMoC with Stable and Turbulent LR-Schedules. Mixing stable and turbulent schedules reaps the most benefit through diversity of learning among different branches.

| LR Regime                                    | $MS \rightarrow C$ |             | $M \rightarrow D$ |             |
|--|--------------------|-------------|-------------------|-------------|
|  | mAP                | R1          | mAP               | R1          |
| Stable ( $\eta = 0.004$ )                    | 29.5               | 29.2        | 50.3              | 67.8        |
| Turbulent ( $\eta = 0.256$ )                 | 27.6               | 26.9        | 50.2              | 68.1        |
| <b>PMoC</b> ( $0.004 \leq \eta \leq 0.256$ ) | <b>30.7</b>        | <b>31.0</b> | <b>51.9</b>       | <b>69.7</b> |

3) *Ablation over weight of DCML:* Table VI compares the effects of different weights of DCML over the benchmarks  $C \rightarrow MS$  and  $C \rightarrow M$ . Setting a loss weight of  $w_3 = 0.01$  yields the most benefit over the control ( $w_3 = 0$ ). With DCML, we observe a performance improvement of around 1-2% in both mAP and Rank-1.

TABLE VI: Ablation over weight of DCML.

| DCML weight ( $\lambda_3$ ) | $C \rightarrow MS$ |             | $C \rightarrow M$ |             |
|-----------------------------|--------------------|-------------|-------------------|-------------|
|                             | mAP                | R1          | mAP               | R1          |
| $w_3 = 0$                   | 16.5               | 39.5        | 52.4              | 74.7        |
| $w_3 = 0.1$                 | 16.8               | 41.0        | 53.4              | 76.0        |
| $w_3 = 0.01$                | <b>17.1</b>        | <b>41.5</b> | <b>54.1</b>       | <b>76.4</b> |
| $w_3 = 0.001$               | 16.4               | 39.9        | 51.8              | 74.4        |

4) *Components of ADP:* Putting the components together, Table VII presents the effects of incrementally adding these components of ADP, demonstrating the gradual improvements contributed by each component.

TABLE VII: Ablation over components of ADP.

| ADP Components |      |      | $C+D+M \rightarrow MS$ |             | MSMT17      |             |
|----------------|------|------|------------------------|-------------|-------------|-------------|
| DyMAIN         | DCML | PMoC | mAP                    | R1          | mAP         | R1          |
|                |      |      | 20.8                   | 44.7        | 56.8        | 79.8        |
| ✓              |      |      | 21.7                   | 45.8        | 59.8        | 81.7        |
|                | ✓    |      | 23.0                   | 50.5        | 60.1        | 81.5        |
|                |      | ✓    | 24.2                   | 52.1        | 59.5        | 82.2        |
| ✓              | ✓    |      | 24.8                   | 50.6        | 60.2        | 83.6        |
| ✓              | ✓    | ✓    | <b>25.7</b>            | <b>53.4</b> | <b>62.0</b> | <b>85.0</b> |

## CONCLUSION

In this paper we investigated the omni-domain generalization capabilities of Person ReID methods and found that methods specialized in one task domain transfer poorly to

other task domains. Although this was broadly within expectations, it was concerning to note that this performance degradation is observed *even if the transfer task is of a simpler setting than the original task*. For example, SOTA multi-source domain generalization methods trained with the full data from the target domain still underperform simple fully supervised baselines. This suggests that such methods are too specialized for their task and do not succeed in varied domain settings. We proposed a novel framework, ADP, to alleviate this overfit. Our method expands a standard backbone architecture into multiple branches, maximizes style differences in the data by applying our proposed normalization method Dynamic Max-Deviance Adaptive Instance Normalization, diversifies per-branch training regimes using our Phased Mixture-of-Cosines learning rate schedules, and aligns interbranch features with our Dimensional Consistency Metric Loss. ADP outperforms recent SOTA methods in DG-ReID as well as in single domain ReID, demonstrating omni-domain generalization and taking a step towards real-world application.

## ACKNOWLEDGEMENTS

This work was supported by the Defence Science and Technology Agency (DSTA) Postgraduate Scholarship, of which Eugene P.W. Ang is a recipient. It was carried out at the Rapid-Rich Object Search (ROSE) Lab at the Nanyang Technological University, Singapore.

## REFERENCES

- [1] H. Luo, Y. Gu, X. Liao, S. Lai, and W. Jiang, "Bag of tricks and a strong baseline for deep person re-identification," in *IEEE Computer Society Conference on Computer Vision and Pattern Recognition Workshops*, vol. 2019-June, pp. 1487–1495, 2019.
- [2] L. Zheng, L. Shen, L. Tian, S. Wang, J. Wang, and Q. Tian, "Scalable person re-identification: A benchmark," in *Proceedings of the IEEE International Conference on Computer Vision*, vol. 2015 Inter, pp. 1116–1124, 2015.
- [3] Z. Zheng, L. Zheng, and Y. Yang, "Unlabeled Samples Generated by GAN Improve the Person Re-identification Baseline in Vitro," in *Proceedings of the IEEE International Conference on Computer Vision*, vol. 2017-October, pp. 3774–3782, 2017.
- [4] W. Li, R. Zhao, T. Xiao, and X. Wang, "DeepReID: Deep Filter Pairing Neural Network for Person Re-identification," in *2014 IEEE Conference on Computer Vision and Pattern Recognition*, pp. 152–159, 2014.
- [5] L. Wei, S. Zhang, W. Gao, and Q. Tian, "Person Transfer GAN to Bridge Domain Gap for Person Re-identification," in *Proceedings of the IEEE Computer Society Conference on Computer Vision and Pattern Recognition*, pp. 79–88, 2018.
- [6] J. Jia, Q. Ruan, and T. M. Hospedales, "Frustratingly easy person re-identification: Generalizing person Re-ID in practice," in *30th British Machine Vision Conference 2019, BMVC 2019*, 2020.
- [7] B. Xu, J. Liang, L. He, and Z. Sun, "Mimic embedding via adaptive aggregation: Learning generalizable person re-identification," in *Computer Vision – ECCV 2022* (S. Avidan, G. Brostow, M. Cissé, G. M. Farinella, and T. Hassner, eds.), (Cham), pp. 372–388, Springer Nature Switzerland, 2022.
- [8] P. Zhang, H. Dou, Y. Yu, and X. Li, "Adaptive cross-domain learning for generalizable person re-identification," in *Computer Vision – ECCV 2022* (S. Avidan, G. Brostow, M. Cissé, G. M. Farinella, and T. Hassner, eds.), (Cham), pp. 215–232, Springer Nature Switzerland, 2022.
- [9] W. Tan, C. Ding, P. Wang, M. Gong, and K. Jia, "Style interleaved learning for generalizable person re-identification," *IEEE Transactions on Multimedia*, 2023.
- [10] A. Dosovitskiy, L. Beyer, A. Kolesnikov, D. Weissenborn, X. Zhai, T. Unterthiner, M. Dehghani, M. Minderer, G. Heigold, S. Gelly, J. Uszkoreit, and N. Houlsby, "An Image is Worth 16x16 Words: Transformers for Image Recognition at Scale," *ICLR 2021*, 2021.

- [11] K. He, X. Zhang, S. Ren, and J. Sun, "Deep residual learning for image recognition," in *Proceedings of the IEEE Computer Society Conference on Computer Vision and Pattern Recognition*, vol. 2016-Decem, pp. 770–778, 2016.
- [12] Y. Huang, J. Xu, Q. Wu, Z. Zheng, Z. Zhang, and J. Zhang, "Multi-pseudo regularized label for generated data in person re-identification," *IEEE Transactions on Image Processing*, vol. 28, no. 3, pp. 1391–1403, 2019.
- [13] S. Lin and C. T. Li, "End-to-End Correspondence and Relationship Learning of Mid-Level Deep Features for Person Re-Identification," in *DICTA 2017 - 2017 International Conference on Digital Image Computing: Techniques and Applications*, vol. 2017-Decem, pp. 1–6, 2017.
- [14] A. Hermans, L. Beyer, and B. Leibe, "In Defense of the Triplet Loss for Person Re-Identification," in *arXiv preprint*, 2017.
- [15] W. Chen, X. Chen, J. Zhang, and K. Huang, "Beyond triplet loss: A deep quadruplet network for person re-identification," in *Proceedings - 30th IEEE Conference on Computer Vision and Pattern Recognition, CVPR 2017*, vol. 2017-Janua, pp. 1320–1329, 2017.
- [16] L. Zheng, Y. Yang, and A. G. Hauptmann, "Person Re-identification: Past, Present and Future," *arXiv preprint*, 2016.
- [17] J. Deng, W. Dong, R. Socher, L.-J. Li, Kai Li, and Li Fei-Fei, "ImageNet: A large-scale hierarchical image database," in *Proc. IEEE Conference on Computer Vision and Pattern Recognition (CVPR)*, pp. 248–255, 2010.
- [18] G. Wang, Y. Yuan, X. Chen, J. Li, and X. Zhou, "Learning discriminative features with multiple granularities for person re-identification," in *MM 2018 - Proceedings of the 2018 ACM Multimedia Conference*, pp. 274–282, 2018.
- [19] M. Ye, J. Shen, G. Lin, T. Xiang, L. Shao, and S. C. H. Hoi, "Deep learning for person re-identification: A survey and outlook," *IEEE Transactions on Pattern Analysis and Machine Intelligence*, 2021.
- [20] X. Pan, P. Luo, J. Shi, and X. Tang, "Two at Once: Enhancing Learning and Generalization Capacities via IBN-Net," in *Lecture Notes in Computer Science (including subseries Lecture Notes in Artificial Intelligence and Lecture Notes in Bioinformatics)*, vol. 11208 LNCS, pp. 484–500, Springer Science+Business Media, 2018.
- [21] X. Huang and S. Belongie, "Arbitrary style transfer in real-time with adaptive instance normalization," in *2017 IEEE International Conference on Computer Vision (ICCV)*, pp. 1510–1519, 2017.
- [22] S. Lin, C.-T. Li, and A. C. Kot, "Multi-Domain Adversarial Feature Generalization for Person Re-Identification," *IEEE Transactions on Image Processing*, nov 2020.
- [23] S. Liao and L. Shao, "Interpretable and Generalizable Deep Image Matching with Adaptive Convolutions," *European Conference on Computer Vision (ECCV)*, vol. abs/1904.1, 2020.
- [24] Y. Zhao, Z. Zhong, F. Yang, Z. Luo, Y. Lin, S. Li, and N. Sebe, "Learning to Generalize Unseen Domains via Memory-based Multi-Source Meta-Learning for Person Re-Identification," in *Proceedings of the IEEE/CVF Conference on Computer Vision and Pattern Recognition (CVPR)*, pp. 6277–6286, jun 2020.
- [25] E. Ang, S. Lin, and A. C. Kot, "DEX: Domain Embedding Expansion for Generalized Person Re-identification," in *The 32nd British Machine Vision Conference*, p. 14, 2021.
- [26] Y. Dai, X. Li, J. Liu, Z. Tong, and L.-Y. Duan, "Generalizable Person Re-identification with Relevance-aware Mixture of Experts," in *2021 Conference on Computer Vision and Pattern Recognition (CVPR)*, may 2021.
- [27] H. Ni, Y. Li, L. Gao, H. T. Shen, and J. Song, "Part-aware transformer for generalizable person re-identification," in *Proceedings of the IEEE/CVF International Conference on Computer Vision*, pp. 11280–11289, 2023.
- [28] K. Zhou, Y. Yang, A. Cavallaro, and T. Xiang, "Learning Generalisable Omni-Scale Representations for Person Re-Identification," in *IEEE Transactions on Pattern Analysis and Machine Intelligence*, 2021.
- [29] E. D. Cubuk, B. Zoph, D. Mane, V. Vasudevan, and Q. V. Le, "Autoaugment: Learning augmentation policies from data," in *Proceedings of the IEEE/CVF Conference on Computer Vision and Pattern Recognition (CVPR)*, 2019.